FULL LENGTH ARTICLE

Mechanisms and models of iridium anomaly shape across the Cretaceous-Paleogene boundary

Pincelli M. Hull[1,2*], Peter J. S. Franks[1], and Richard D. Norris[1]

[1]*Scripps Institution of Oceanography, University of California at San Diego, La Jolla, CA 92093*

[2]*Present Address: Department of Geology and Geophysics, Yale University, New Haven, CT 06520*

* To whom correspondence should be addressed. Yale Department of Geology and Geophysics, PO Box 208109, New Haven, CT 06520-8109; tel. 858 822-2783; fax 203-432-3134; E-mail: pincelli.hull@yale.edu

Abstract

The interpretation of the Cretaceous-Paleogene (K-Pg) iridium anomaly – and other impact ejecta – as the result of a single, large asteroid impact has been the subject of much debate, in part due to the distribution of impact markers beyond the narrow confines of the K-Pg boundary sedimentary layer. Here, we revisit the hypothesized processes leading to the shape of K-Pg iridium profiles including geochemical remobilization and/or diffusion, prolonged deposition, volcanism, multiple impacts, and sediment mixing. Using evidence from the literature and modeling of one North Pacific site, we find that sediment mixing of a single impact event provides the most parsimonious mechanism for iridium profile shape in open ocean oxic sediments, while the increase in background iridium bracketing the boundary likely has a volcanic origin. In some past studies, a sediment mixing mechanism for iridium profile shape was ruled out based on an overly simplified set of expectations for the effect of sediment mixing on markers of geologically instantaneous events. Thus, we introduce and use a Lagrangian sediment-mixing model to illustrate the theoretical effects of mixing on records of rapid events. The sediment mixing origin for iridium anomaly shape, the correspondence in mixing extent between iridium and microfossils, and the fit of sediment mixing models to an empirical iridium profile indicate that iridium may provide a better tracer of mixing than previously proposed K-Pg mixing tracers such as Ni-spinels.

Keywords

K/Pg boundary, impact ejecta, bioturbation, PGE, advection-diffusion model, fossil record preservation

1. Introduction

An extraterrestrial impact like that at the Cretaceous-Paleogene (K-Pg) boundary results in the rapid deposition of a number of physical and chemical markers of the event (Kyte 2002) , including iridium (Ir) and other platinum group elements (PGEs), shocked quartz, nickel-spinels, microtektites, and microkrystites (as reviewed in Alvarez 1996, Smit 1999, Claeys et al. 2002). Impact markers like iridium are primarily deposited in thin, <<1 cm thick, event horizons at distal sites (Smit 1999, Claeys et al. 2002) before being remobilized by sedimentary processes like bioturbation, geochemical remobilization or slumping. The cumulative affect of sedimentary processes is preserved in the fossil record by the shape of the concentration profile of the impact marker (e.g., the depth distribution of the material initially deposited in a single layer). As a result, geologically instantaneous markers like impact ejecta and volcanic ashes have long been used to quantitatively understand deep-sea sediment mixing (e.g., Glass 1969, Ruddiman and Glover 1972, Guinasso and Schink 1975, Ruddiman et al. 1980). Concentration profiles of event markers can be used to quantify the magnitude and duration of the initial, unmixed record of both the impact marker and other sedimentary constituents like foraminifera, diatoms, and other nanofossils (Ruddiman and Glover 1972).

At the K-Pg boundary a number of questions exist about the ecological, evolutionary, and biogeochemical response in the decades to millennia following the impact, as most sediment records are well mixed over these time scales. However, despite an abundance of impact markers and the potential utility of mixing models to quantify the effects of sediment mixing, we are unaware of any previous attempt to use models to test hypotheses concerning sediment mixing across the K-Pg boundary. Iridium anomalies at the K-Pg boundary have the potential to be useful tracers of sedimentary mixing as they were deposited in a geologically brief interval and have been measured at more sites and at a higher resolution than other K-Pg impact markers

(Claeys et al. 2002). However, to be useful for such studies, the shape of iridium anomalies must be primarily determined by sedimentary mixing and representative of the effect of sediment mixing on other sedimentary constituents of interest, like marine microfossils.

Here, we address two issues. First, does the shape of vertical profiles of iridium anomalies primarily reflect sediment mixing in oxic, pelagic sites distal to the impact or does it primarily reflect other processes, like geochemical remobilization or volcanism? The shape of the iridium anomaly – a peak with asymmetric up-core and down-core tails – has been attributed to a number of sedimentary processes (e.g., Smit 1999, Stueben et al. 2002) including: i) bioturbation and other sedimentary mixing processes like slumping (Kyte et al. 1985, Alvarez et al. 1990), ii) diagenetic remobilization and diffusion (Kyte et al. 1985, Schmitz 1985, Wallace et al. 1990), iii) prolonged deposition due to oceanic residence time of dissolved K-Pg impactor iridium (Anbar et al. 1996), iv) prolonged deposition due to volcanism (Officer and Drake 1985, Crocket et al. 1988, Rocchia et al. 1990), v) multiple impacts (Keller et al. 2003, Stuben et al. 2005), and vi) redeposition from primary deposits (Preisinger et al. 1986). Of these, only the first five provide a global mechanism for shaping iridium anomalies. We evaluate evidence for each mechanism in the literature and by modeling a highly resolved iridium anomaly in the North Pacific (Shatsky Rise).

Second, we examine the theoretical range of effects that sediment mixing can have on records of geologically instantaneous events. Here, we discuss issues that are well-known within the sediment mixing community but that are sometimes missed in the interpretation of the distribution of K-Pg boundary markers. These include the effects of lumpy mixing, sediment grain size, and changing mixing intensity or depth. We illustrate these effects by examining empirical K-Pg boundary records and by modeling iridium anomalies under a range of theoretical mixing conditions with a Lagrangian advection-diffusion sediment-mixing model.

2. Mixing model

Here, we introduce and use a Lagrangian particle-tracking model of sediment mixing, which uses a stochastic algorithm to move material based on vertically varying diffusivities. Our non-deterministic approach has several distinct advantages over deterministic mixing models: i) it directly allows for the calculation confidence limits on concentration profiles, ii) since concentrations are not calculated on a spatial grid, it removes the problem of concentrations diffusing unrealistically quickly through the domain, and iii) it can be readily modified to incorporate random processes like lumpy mixing.

The simplest and most widely used sediment mixing models are advection-diffusion models. In an advection-diffusion model, the record of a sedimentary event is distributed within a mixed layer according to a mixing coefficient (e.g., diffusion coefficient), while being advected into a historic layer of sediment that predates the event (Goldberg and Koide 1962, Guinasso and Schink 1975). Typically, concentrations of a property are calculated at fixed grid points (e.g., depths), leading to systematic numerical errors and numerical diffusion. Basic advection-diffusion approaches generally do not model non-local mixing like the lumpy mixing of large burrowers that occasionally carry surface sediment to great depths (Smith et al. 1986). While non-local sediment mixing models do exist (e.g., Boudreau and Imboden 1987, Trauth 1998, Shull 2001), they are difficult to parameterize from tracer profiles alone (Boudreau 1986a, b, Boudreau and Imboden 1987) and do not necessarily outperform advection-diffusion models (Meysman et al. 2003).

Our model is a one-dimensional Lagrangian particle-tracking model with a depth-dependent eddy diffusivity modified from Tanaka and Franks (2008). Sediment mixing was driven by vertical diffusivity (K_v), which we modeled as a decreasing hyperbolic tangent (*tanh*) function (Fig. 1). The *tanh* function captures a fundamental feature of sediment mixing, namely, the existence of a superficial well-mixed layer underlain by increasingly unmixed sediments. The *tanh* function generates a vertical diffusivity profile that is continuously differentiable with depth – a property that is desirable for modeling depth-dependent diffusivities (Ross and Sharples 2004). The depth of sediment mixing and diffusivity are expected to primarily be a function of the flux of organic matter to the deep sea (e.g., Trauth et al. 1997, Smith and Rabouille 2002), and are used here as free parameters for tuning the mixing model to fit measured iridium anomalies.

Three parameters define sediment mixing: i) z_0 is the depth of the inflection point in the *tanh* profile, delineating the bottom of the well-mixed layer of sediment, ii) z_{scale} is the *e*-folding scale for the *tanh* profile and determines the depth over which mixing asymptotes to zero, and iii) K_0 is the maximum vertical diffusivity. K_v, or depth-dependent diffusivity, decreases with depth according to:

$$K_v(z) = \frac{K_0}{2}\left[1 - \tanh\left(\frac{z - z_0}{z_{scale}}\right)\right]$$

Unlike many mixing models, K_0 defines the upper limit of mixing in the *tanh* profile, and not diffusivity at the sediment-water interface. As z_{scale} approaches zero, the diffusivity at the sediment-water-interface ($K_{surface}$) will approach K_0 (Fig. 1 grey versus black line).

Modeled iridium was moved vertically by vertical diffusivity after the algorithms of Visser (1997) and Ross and Sharples (2004), as a Markov process where the depth $z_{t+\Delta t}$ of a particle at time $t+\Delta t$ was a function of the depth (z_t) in the previous time step (t):

$$z_{t+\Delta t} = z_t + \frac{\partial K_v(z_t)}{\partial z}\Delta t + R\left[\frac{2K_v(z_t + \frac{1}{2}\frac{\partial K_v}{\partial z}\Delta t)\,\Delta t}{r}\right]^{1/2} + w_s\Delta t$$

where R is a random process with a zero mean and a variance of r. We set $r = 1/3$, and drew R from a uniform distribution ranging from -1 to 1 (Ross and Sharples 2004, Tanaka and Franks

2008). Sedimentation (w_s) drives the continual sinking of sediment out of the mixed layers. The mixing model time step Δt was 10 years, representing a compromise between model run-time and an accurate depiction of mixing.

Iridium deposition was simulated by the introduction of "particles" into the model at the sedimentary surface, with each particle representing an equal amount of iridium. 10,000 and 100,000 particles were injected into the model and mixed according to the model parameterization in order to fit empirical iridium profiles and explore mixing model sensitivity respectively. Particle numbers were binned over 0.2 cm deep increments to obtain concentrations; the magnitude of the iridium anomaly was matched by multiplying the modeled profile by a constant. Model simulations were repeated 100 times during empirical model fitting, as individual model runs can vary due to the non-deterministic nature of our approach. Model fit is reported as the r^2 between the median model and measured iridium. We included 36 data points in the calculation of r^2, truncating the long tails of background measurements as our model does not include any background iridium.

We approximate a one-layer model to contrast with the *tanh*-profile model by setting z_{scale} equal to 1.5 cm. This small value of z_{scale} approximates a surface well-mixed layer, but allows the simulation to model the bottom boundary without a large boundary artifact (Ross and Sharples 2004). In general, model artifacts are introduced when:

$$\Delta t \lesssim \frac{(z_{scale})^2}{2K_0}$$

When Δt is equal to or larger than this ratio, the model will generate artificial accumulations of particles along boundaries (Ross and Sharples 2004).

We model the sediment-sea water interface as a reflecting boundary to handle instances where modeled sediment would be moved above the sea floor. The values of K_0, z_0, and z_{scale}

were fit through an iterative procedure. In practice, we explored the model parameter space to identify promising parameter combinations. K_0, z_0, and z_{scale} were then optimized by randomly combining parameters drawn from uniform distributions in parameter space centered around initial K_0, z_0, and z_{scale} values. The best parameter combination was selected as the one that minimized the absolute average error (Stow et al. 2009).

3. Theoretical modeling experiments

The first three modeling experiments explored the effect of varying a single model parameter on modeled profile shape, while holding all other parameters constant. K_0, or diffusivity, was explored from 1-100 cm^2/kyr in the mixing rate experiment (Fig. 2a), resulting in profiles with varying up-core slopes, in contrast to similar down-core profiles. The highest diffusivities corresponded to the widest spread in boundary iridium and the most gradual up-core slope. Varying sedimentation rate, w_s, from 0.5-15 cm/kyr (Fig. 2b) changed iridium profile symmetry in addition to up-core and down-core iridium anomaly width and slope. Higher sedimentation rates, 5 and 15 cm/kyr, resulted in relatively symmetrical and narrow iridium anomalies as compared to profiles obtained with sedimentation rates of 0.5 and 1 cm/kyr. Varying the mixing depth, z_0, from 2-15 cm changed the extent of down-core mixing (Fig. 2c). Deep mixing (large z_0) increased the depth of the down-core tail, while increasing overall profile symmetry.

We used a no-mixing experiment to test the hypothesis that the deposition (via scavenging) of dissolved iridium was sufficient to account for the shape of K-Pg boundary anomalies. On impact, part of the K-Pg bolide was vaporized, delivering a portion of the original iridium in a dissolved rather than particulate state (Paquay et al. 2008). We modeled multiple impactor vaporization scenarios with the assumption of no sedimentary mixing in order to visualize the sensitivity of the iridium peak to the large uncertainties in both the portion of the impactor vaporized (10-70% vaporization was tested) and the range of residence times for dissolved oceanic iridium (2,000-20,000, Anbar et al. 1996, Fig. 2d). We found that impactor dissolution alone resulted in very little spread in the boundary iridium even with the most permissive assumption (Fig. 2d). In addition, at the sedimentation rates typical of early Paleocene open ocean sites (0.5 - 1 cm/1000 years), the prolonged input of iridium had a minimal effect on profile shape after sediment mixing (Fig. 2e mixing scenario 1, between profile r^2=0.99, p< 0.001), as well as on model parameterization and fit.

In mixing scenario 2, we explored the possible complexity of iridium profiles that could be obtained given assumptions of temporally heterogeneous mixing depths and intensities, and the prolonged deposition of iridium following the K-Pg impact (Fig. 2f). Specifically, we modeled a large increase in mixing depth and intensity for 50 years following the K-Pg impact. This boundary mixing spike model was parameterized with base parameters of K_0= 1.0 cm^2/kyr, z_0= 5 cm, z_{scale}= 1.5 cm, w_s= 0.5 cm/kyr, and a 50 year period of enhanced mixing beginning with the iridium injection with parameters of K_0= 1000 cm^2/kyr, z_0= 100 cm, z_{scale}= 1.5 cm, w_s= 0.5 cm/kyr. Iridium deposition assumptions included the 30% dissolution of the impactor, a 6,300 year oceanic residence time for dissolved iridium, and a 60 year residence time for particulate iridium. Figure 2f demonstrates one example of the effect of temporally heterogeneous mixing and prolonged iridium deposition, and approximates the shape complexity that can be observed in heavily bioturbated sites such as Maud Rise (Fig. 3a).

4. Sample materials

We fit a highly resolved iridium anomaly measured by Michel et al. (1985) at the Deep Sea Drilling Program (DSDP) Site 577B, Shatsky Rise, North Pacific (32°26.48'N, 157°43.39'E) (Heath et al. 1985). The biostratigraphically complete K-Pg boundary section was described as "a slightly mottled nanofossil ooze", with mottling of the boundary reflecting the bioturbation of the very pale brown Danian sediments into the white upper Maastrichtian nanofossil ooze (Heath et al. 1985). We inferred sedimentation rates for DSDP Site 577B by tuning an x-ray florescence (XRF) record of Fe to a nearby astronomically calibrated site, Ocean Drilling Program (ODP) Site 1211. ODP Site 1211 was astronomically calibrated through the Paleocene to a number of sites by Westerhold et al. (2008), providing the most reliable set of relative ages for calculating sedimentation rates at Site 577B (see Supplemental Table s1 and s2 for age model and age model tie points). In addition to fitting sediment mixing models to measured iridium anomalies, we also considered the distributions of three additional elements measured by Michel et al. (1985) as proxies for diagenetic remobilization: Fe, Ni, and Al.

5. Determinants of K-Pg iridium anomaly shape in open ocean sediments

5.1 Evidence for the diagenetic remobilization of iridium

Among the siderophilic elements enriched in K-Pg boundary sediments, iridium is the best candidate for a tracer of mixing as it is the least likely to be diagenetically remobilized (Colodner et al. 1992, Evans et al. 1993), and unlikely to be confounded by other iridium sources (Kyte 2002). Although relatively immobile, recent work has shown that iridium like other PGEs can be mobilized in reducing, low-temperature pore fluids (Colodner et al. 1992, Evans et al. 1993, Sawlowicz 1993). For example, remobilization of iridium in recent pelagic sediments under changes in redox conditions has been studied in an abyssal plain periodically influenced by distal turbidite flows (Colodner et al. 1992). Iridium becomes mobile by the reduction of oxic sediments below a newly deposited turbidite, resulting in a depletion of iridium at the oxic/suboxic transition (Colodner et al. 1992). This mechanism cannot account for the larger iridium anomalies at the K-Pg boundary, but has been evoked to explain iridium anomalies in other intervals marked by a large change in sedimentary environments and redox conditions (Wallace et al. 1990, Colodner et al. 1992, Sawlowicz 1993, Wang et al. 1993). There is evidence, however, for the remobilization of the K-Pg boundary iridium anomaly in reducing environments, including terrestrial coal deposits (Izett 1990, Evans et al. 1993) and, possibly, reducing marine settings (Martinez-Ruiz et al. 1999). Remobilization of iridium in reducing K-Pg sediments is not a universal feature, as iridium can lack evidence of remobilization in reducing sites where other PGEs are remobilized (Evans et al. 1993, Kyte 2002) and PGE ratios often differ from expected values given their relative diagenetic mobility (e.g., Stueben et al. 2002, Lee et al. 2003).

Pelagic sections have relatively low organic carbon content and, outside of the Tethys and other neritic sites, appear to have been largely oxic in the early Danian (e.g., Perch-Nielsen et al. 1977, Heath et al. 1985, Barker et al. 1988). Indeed, the sites that we have investigated largely have tan, pink, or reddish brown colors in boundary sediments indicating oxic conditions in both the Maastrichtian and the early Paleocene. Oxic bottom waters and low organic fluxes are both characteristics which theoretically reduce the likelihood of iridium remobilization (e.g., Colodner et al. 1992). Thus, while iridium remobilization has been observed in reducing environments, diagenetic remobilization of K-Pg boundary iridium is relatively unlikely in oxic pelagic sediments.

5.2 Evidence for prolonged deposition shaping deep sea iridium profiles

The spread in the iridium anomaly at the K-Pg boundary has also been attributed to prolonged iridium input from the partial dissolution of the impactor (Anbar et al. 1996, although see Smit 1999), with subsequent deposition through scavenging from surface waters. We were unable to simulate a comparable spread in the iridium anomaly by simply assuming a prolonged iridium input (Fig. 2d) with very permissive assumptions including a higher impactor dissolution than has previously been hypothesized (70% in contrast to the 5-30% typically considered, Paquay et al. 2008), the uppermost bound for iridium residence times (20 kyr, Anbar et al. 1996), and low sedimentation rates (0.5 cm/kyr). From this we conclude that the shape of K-Pg boundary iridium anomalies are unlikely to be strongly influenced by the prolonged deposition of dissolved impact iridium.

5.3 Evidence of volcanism in deep sea iridium profiles

Many K-Pg iridium profiles have low, wide shoulders bracketing the steep boundary anomaly with iridium concentrations above background levels (e.g., Officer and Drake 1983, Rocchia et al. 1990, Robin et al. 1991). This enrichment above background iridium, readily apparent only on a log scale, has been variously attributed to volcanism (Officer and Drake 1985, Rocchia et al. 1990), multiple impacts (Rocchia et al. 1990), prolonged iridium input (Anbar et al. 1996), a change in sedimentary dilution (Robinson et al. 2009), and diagenetic remobilization of iridium (Rocchia et al. 1990, Robin et al. 1991). Growing evidence suggests that Deccan volcanism may provide the most parsimonious explanation for this increase in background iridium.

The time period of the main phase of Deccan volcanism generally coincides with a pre- and post-boundary elevation in background iridium. Peak Deccan emplacement occurred during C29r which lasted ~800 kyr (Courtillot et al. 1986), with the main volcanic phase beginning ~340 kyr prior to the impact (Robinson et al. 2009) and possibly ending at the K-Pg boundary with a subsequent eruption in late C29r to early C29n (Chenet et al. 2007, Keller et al. 2009). The increase in background iridium spans a comparable time interval at some sites (e.g., Rocchia et al. 1990, Robin et al. 1991, Robinson et al. 2009), although it appears considerably shorter at others (Officer and Drake 1985, Robin et al. 1991). Osmium isotopes and osmium and iridium levels at multiple sites indicate a distinct pre-boundary shift coincident with the onset of Deccan volcanism (Ravizza and Peucker-Ehrenbrink 2003, Robinson et al. 2009), with PGE ratios (Pt/Ir) ruling out extensive diagenetic remobilization. Deccan volcanism may influence iridium, osmium and other PGEs directly by the addition of new PGEs to the ocean or indirectly via decreased sedimentation rates due to acidification from volcanogenic CO_2 (Robinson et al. 2009).

Alternative mechanisms for the increase in background iridium fail to fully explain the observed patterns: i) slow deposition of dissolved impact iridium cannot account for the pre-impact elevation in background concentrations, ii) diagenetic explanations have been rejected in a recent investigation on the basis of Pt/Ir ratios (Robinson et al. 2009), evidence which also precludes a sediment mixing mechanism, and iii) evidence for multiple impacts as a source of the background iridium profile is lacking as small iridium peaks occur at different stratigraphic intervals between cores (Fig 4a,b) and correspond with burrows within cores (Fig. 4, and see Pospichal et al. 1990). Thus, the relative timing and explanatory power suggests that Deccan volcanism accounts for the increase in background iridium.

5.4 Evidence for multiple impacts in deep-sea iridium profiles

Arguments have been made for multiple impacts at the K-Pg boundary on the basis of the relative distribution of iridium and impact ejecta (Keller et al. 2003, Stuben et al. 2005, and references therein) and, recently, a second impact crater of near-Chicxulub age (Jolley et al. 2010). In the first case, authors argue for at least two impacts based on the stratigraphic distribution of iridium and impact ejecta in the Gulf of Mexico (Keller et al. 2003, Stuben et al.

2005), with one hypothesized impact preceding the K-Pg boundary by ~300,000 years and one at or ~100, 000 years subsequent to the K-Pg boundary. These authors justify the consideration of iridium and other impact eject exclusively from sites adjacent to the Chicxulub impact crater on the grounds that open ocean sediments would not resolve multiple impacts separated by 300-400 kyrs, given the presence sediment mixing and low sedimentation rates (Keller et al. 2003). However, empirical evidence does not support the exclusion of distal, pelagic sites from consideration. In the North Pacific sites at Shatsky Rise, iridium from a 300 kyr pre K-Pg impact should appear – but does not – at approximately -300 cm relative depth (Fig. 4b), well outside the depth spanned by the mixed K-Pg iridium anomaly. The same is true in the Indian Ocean core at ODP Site 761C, where the 300kyr pre K-Pg iridium anomaly is not detected, or obscured, at approximately -187 cm relative depth (Fig. 4a). Thus, iridium anomaly shape in distal, pelagic sites provides evidence against the multiple impact hypotheses (see Schulte et al. 2010, and references therein for the alternative hypothesis for complex Gulf stratigraphy).

In contrast, the recently proposed age of the Boltysh impact crater, 2-5 kyr pre-Chicxulub (Jolley et al. 2010), cannot be tested by typical pelagic iridium anomalies, due to the relatively small size of the Boltysh impactor and short hypothesized period between impacts.

5.5 Evidence for sediment mixing from the shape of boundary anomalies

From the earliest discussions of the distribution of boundary ejecta and microfossils, bioturbation and other sedimentary processes have been used to explain the apparent temporal spread of impact markers and the faunal mixing of the late Cretaceous and early Paleocene species (e.g., Thierstein 1981, Kyte et al. 1985, Robin et al. 1991). Pervasive burrowing of complete distal K-Pg boundary sections is readily apparent due to a distinct color change between light Maastrichtian and dark Danian sediments (Smit 1999). Among the visibly bioturbated boundary sections are sites like Agost (Rodriguez-Tovar 2005), Caravaca (Rodriguez-Tovar and Uchman 2008), and Maud Rise (Pospichal et al. 1990), to name just a few. Burrowing by early Danian benthic communities into Masstrichtian sediments is confirmed by the presence of impact ejecta (Rodriguez-Tovar 2005) and Danian fossils (e.g., Pospichal et al. 1990, Premoli Silva et al. 2005) in the boundary-crossing burrows. The correspondence between the extent of visible burrows, fossil reworking, and the iridium anomalies at sites like Maud Rise (Fig. 3a, Barker et al. 1988, Michel et al. 1990) and El Kef (Robin et al. 1991, Pospichal 1994), and the extent of coring disturbance and the iridium anomaly at Hess Rise (Fig. 3b, Michel et al. 1981, Vallier et al. 1981), provides some support for the hypothesis that sediment mixing is the primary determinant of iridium anomaly shape in oxic, pelagic sites distal to the impact.

The correspondence in mixing extent between iridium and microfossils suggests that iridium has a key characteristic of a useful tracer: it tracks the mixing of other sedimentary constituents. Sediment mixing is generally biased by size, with smaller particles being transported over greater distances than larger particles (e.g., Wheatcroft 1992, Thomson et al. 1995, although see McCave 1988). In a comparison between boundary profiles of iridium and Ni-spinels, iridium anomalies had greater peak widths than Ni-spinels in the three sites analyzed (Robin et al. 1991). Ni-spinels are much larger (Robin et al. 1991 quantified spinels >1 mm) and denser than the main constituents of carbonate oozes (foraminifera, nanoplankton, and clay). In contrast, iridium is thought to be bound to the clay or fine fraction of sediments (Rocchia et al. 1990, Claeys et al. 2002). A comparison between nanofossil reworking (Pospichal 1994) and the up-core tail of iridium at El Kef (Robin et al. 1991), indicates that iridium provides a better tracer than Ni-spinels of the sedimentary mixing of nanofossils. The Ni-spinel peak at all sites studied by Robin et al. (1991) is thin compared to typical burrowing depth and fossil reworking as well as iridium anomaly width, suggesting that iridium may behave more like the carbonate fossils that comprise most of the sediment.

In some pelagic sites, sediment mixing has been displaced by chemical remobilization as a hypothesis explaining iridium anomaly shape on the grounds of an overly symmetrical anomaly shape (e.g., Officer and Drake 1985, Lee et al. 2003) and a thickness (uncompacted thickness of 61 cm at DSDP Site 384, North Atlantic) requiring an unrealistically large mixing depth (Officer and Drake 1983). However, our results show that realistic mixing depths and rates can readily generate anomalies with comparable dimensions (Fig. 2).

6. Test of sediment mixing hypothesis in North Pacific

Diagenetic remobilization and prolonged iridium inputs do not appear to explain much of the shape in K-Pg boundary iridium at North Pacific DSDP Site 577B, Shatsky Rise. Fe, Ni, and Al anomalies match the iridium anomaly shape despite the range in susceptibility of these elements to geochemical remobilization in reducing environments (Fig. 5a). We would expect diagenetic remobilization to cause the divergence of elemental profiles from one another as Al is relatively resistant to geochemical remobilization compared to Ni and Fe, but this is not observed. Similarly, modeled prolonged iridium input from impact vaporization alone poorly fits the observed iridium shape (Fig. 5b, r^2=0.12, p=0.04). Without mixing, 70% of the iridium input is contained in 3 cm spanning the K-Pg boundary, compared with the approximately 20 cm spanned by 70% of the boundary iridium at DSDP Site 577B.

In contrast to geochemical remobilization and prolonged iridium input, our Lagrangian advection-diffusion mixing models explain most of the observed iridium anomaly shape (Fig. 5c-d, r^2= 0.95 and p< 0.001). As a general note, reliably fitting sediment mixing models to iridium anomalies like that in the North Pacific requires i) densely sampled records of the anomaly to avoid model overfitting, and ii) large enough anomalies to have a high signal-to-noise ratio, given the difficulty of precisely measuring low, background iridum concentrations.

The mixing model failed to fit two Maastrichtian peaks between 75 and 85 cm. Late Cretaceous sedimentation rates for this site (1 cm/kyr from the initial site report, Heath et al. 1985) suggest that these peaks could have occurred between 75 and 85 kyr before the K-Pg boundary if they are assumed to represent pre-boundary inputs of iridium. However, given the distinct mottled appearance of boundary mixing (Fig. 5a) and the lack of correspondence of secondary peaks with other cores from the same locale (Fig. 4b), we suspect that both peaks are due to lumpy mixing rather than pre-boundary events. These pre-boundary peaks highlight a general limitation of basic advection-diffusion models; namely, they are not designed to model non-local mixing like the rare transport of surface sediment to great depths by large burrowers. However, Lagrangian mixing models such as ours could be configured to include lumpy mixing.

7. General expectations for mixed records of rapid events

The theoretical modeling experiments, literature review, and analysis at the Shatsky Rise, North Pacific emphasize a number of general expectations for mixed records of geologically instantaneous events like the impact at the K-Pg boundary.

1) **Strict tests of profile symmetry cannot be used to test for sediment mixing.** Sediment mixing can spread a point event into a wide range of profile shapes from relatively symmetric to down-core tailing under assumptions of no-change in mixing depth or rate, to up-core tailing with assumptions of decreased mixing rates with the time (Fig. 2).

2) **For any event, small sedimentary constituents may be transported farther than large ones.** The differential reworking of nanofossils and foraminifera across the K-Pg boundary, and different K-Pg boundary placement on the basis of

iridium, nanofossil and foraminiferal biostratigraphy have all been the subject of some debate in the past. Such offsets are expected given sediment mixing. The relative depth of sediment mixing can range from effectively the same across size classes to increasing with decreasing size from foraminifera to nanofossils to iridium. The largest sedimentary constituents (Ni-spinels and other large ejecta at the K-Pg boundary) will typically have narrow distributions compared to all common pelagic sedimentary constituents.

3) **Sediment mixing tends to move the peak depth of a mixing tracer into stratigraphically older sediments.** The relative magnitude of the peak offset from the depth of initial emplacement is controlled by the combination of mixing parameters used to generate a given concentration profile. The depth of peak shift can be as the depth of the weighted mean of a given concentration profile (e.g., Guinasso and Schink 1975), but is sensitive to factors like lumpy mixing and changing mixing intensity through time. As an alternative, it may be possible to estimate shift by a comparison of relatively immobile particles like large ejecta and relatively mobile particles like sediment-associated iridium. Both methods could be used to constrain the possible mixing parameter combinations to better approximate the mixing conditions that generated a given profile.

4) **Lumpy or non-local mixing can result in secondary peaks in the abundance of an event marker; peaks may not occur at all locales, will be diachronous when present, and may visibly correspond with displaced sediment.** Advection-diffusion models, including the model used in this study, typically do not model non-local, lumpy mixing. However, at the K-Pg boundary secondary peak characteristics fit the description above suggesting that lumpy mixing provides a reasonable explanation for secondary peaks in K-Pg iridium anomalies when present.

5) **If a chemical marker is transported to depths equal to or less than the depth of visible burrowing, then sediment mixing may provide the most parsimonious determinant of profile shape.** Although geochemical

remobilization and diffusion are commonly evoked to explain K-Pg iridium profiles in the presence of visible burrowing, it is difficult to imagine conditions in which mixing would move sediment but not iridium, with diagenetic remobilization of iridium only occurring once sediment sinks below the depth of active mixing. Sediment mixing is not always visible, so the converse of this statement is not valid.

8. Conclusions

The shape of the K-Pg iridium anomaly in oxic, pelagic sites appears to be primarily determined by sediment mixing. Evidence supporting sediment mixing includes: (1) the correspondence of iridium profiles with sedimentary burrows and boundary material, (2) the low mobility of iridium in oxic sediments, and (3) the similarity of element profiles despite differences in susceptibility to geochemical remobilization. Many existing studies attribute the shape of the iridium anomaly to geochemical remobilization by default, despite the extensive documentation of burrowing and evidence for assemblage mixing across the boundary. We find more evidence supporting remobilization of iridium in reducing sites and advise against the use of iridium as a mixing tracer in these instances.

We directly modeled sediment mixing at Shatsky Rise by fitting a Lagrangian advection-diffusion model to measured iridium and found that our simplest model provided the best fit relative to model complexity. Thus, parameterizing sediment-mixing models to K-Pg boundary iridium anomalies offers a powerful approach for quantitatively defining and accounting for the extent of mixing effects in K-Pg boundary records. It remains to be tested whether mixing models can fit highly resolved iridium anomalies from other pelagic environments with more complicated mixing histories. If sediment-mixing models can be fit to a range of pelagic boundary sections, it may be possible to statistically increase the temporal resolution of our interpretation of boundary impacts and recovery in the earliest Danian.

Acknowledgements

This work was supported by a NASA grant to R. Norris and in part by the Yale University Faculty of Arts and Sciences High Performance Computing facility and staff. Our research relied on records and studies supported by the Ocean Drilling Program (Deep Sea Drilling Project). We thank M. Ohman for manuscript suggestions and Brian Dobbins for technical support on the use of Yale computing resources.

Appendix A. Supplementary data

Supplementary data associated with this article can be found, in the online version, at _.

References

Alvarez, W., 1996. Trajectories of ballistic ejecta from the Chicxulub Crater. Geol. Soc. Am. Spec. Pap. 307, 141-150.

Alvarez, W., et al., 1990. Iridium profile for 10-million years across the Cretaceous-Tertiary boundary at Gubbio (Italy). Science 250, 1700-1702.

Anbar, A.D., et al., 1996. Iridium in natural waters. Science 273, 1524-1528.

Barker, P.F., et al., 1988. Site 690. Proc. Ocean Drill. Prog. Init. Repts. 113, 183-292.

Boudreau, B.P., 1986a. Mathematics of tracer mixing in sediments: 1. Spatially-dependent, diffusive mixing. Am. J. Sci. 286, 161-198.

Boudreau, B.P., 1986b. Mathematics of tracer mixing in sediments: 2. Nonlocal mixing and biological conveyor-belt phenomena. Am. J. Sci. 286, 199-238.

Boudreau, B.P., Imboden, D.M., 1987. Mathematics of tracer mixing in sediments: 3. The theory of nonlocal mixing within sediments. Am. J. Sci. 287, 693-719.

Chenet, A.L., et al., 2007. K-40-Ar-40 dating of the Main Deccan large igneous province: Further evidence of KTB age and short duration. Earth Planet. Sci. Lett. 263, 1-15.

Claeys, P., et al., 2002. Distribution of Chicxulub ejecta at the Cretaceous-Tertiary boundary. Geol. Soc. Am. Spec. Pap. 356, 55 - 69.

Colodner, D.C., et al., 1992. Postdepositional mobility of platinum, iridium and rhenium in marine-sediments. Nature 358, 402-404.

Courtillot, V., et al., 1986. Deccan flood basalts at the Cretaceous-Tertiary boundary. Earth Planet. Sci. Lett. 80, 361-374.

Crocket, J.H., et al., 1988. Distribution of noble-metals across the Cretaceous/Tertiary boundary at Gubbio, Italy - iridium variation as a constraint on the duration and nature of Cretaceous/Tertiary boundary events. Geology 16, 77-80.

Evans, N.J., et al., 1993. Ru/Ir Ratios at the Cretaceous-Tertiary boundary - Implications for PGE source and fractionation within the ejecta cloud. Geochim. Cosmochim. Acta 57, 3149-3158.

Glass, B.P., 1969. Reworking of deep-sea sediments as indicated by vertical dispersion of Australasian and Ivory Coast microtektite horizons. Earth Planet. Sci. Lett. 6, 409-415.

Goldberg, E.D., Koide, M., 1962. Geochronological studies of deep sea sediments by the ionium/thorium method. Geochim. Cosmochim. Acta 26, 417-450.

Guinasso, N.L., Schink, D.R., 1975. Quantitative estimates of biological mixing rates in abyssal sediments. J. Geophys. Res.-Oc. Atm. 80, 3032-3043.

Heath, G.R., et al., 1985. Site 577. Init. Repts. Deep Sea Drill. Prog. 86, 91-137.

Izett, G.A., 1990. The Cretaceous/Tertiary boundary interval, Raton Basin, Colorado, and New Mexico, and its content of shock-metamorphosed minerals: evidence relevant to the K/T boundary impact-extinction theory. Geol. Soc. Am. Spec. Pap. 249, 100.

Jolley, D., et al., 2010. Two large meteorite impacts at the Cretaceous-Paleogene boundary. Geology 38, 835-838.

Keller, G., et al., 2009. K-T transition in Deccan Traps of central India marks major marine seaway across India. Earth Planet. Sci. Lett. 282, 10-23.

Keller, G., et al., 2003. Multiple impacts across the Cretaceous-Tertiary boundary. Earth-Sci. Rev. 62, 327-363.

Kyte, F.T., 2002. Tracers of the extraterrestrial component in sediments and inferences for Earth's accretion history. Geol. Soc. Am. Spec. Pap. 356, 21-38.

Kyte, F.T., et al., 1995. Identification and characterization of the Cretaceous/Tertiary boundary at ODP Sites 886 and 803 and DSDP Site 576. Proc. Ocean Drill. Prog. Sci. Results 145, 427-434.

Kyte, F.T., et al., 1985. Siderophile interelement variations in the Cretaceous-Tertiary boundary sediments from Caravaca, Spain. Earth Planet. Sci. Lett. 73, 183-195.

Lee, C.T.A., et al., 2003. Platinum-group elements (PGE) and rhenium in marine sediments across the Cretaceous-Tertiary boundary: constraints on Re-PGE transport in the marine environment. Geochim. Cosmochim. Acta 67, 655-670.

Martinez-Ruiz, F., et al., 1999. Positive Eu anomaly development during diagenesis of the K/T boundary ejecta layer in the Agost section (SE Spain): implications for trace-element remobilization. Terr. Nova 11, 290-296.

McCave, I.N., 1988. Biological Pumping Upwards of the Coarse Fraction of Deep-Sea Sediments. J. Sediment. Petrol. 58, 148-158.

Meysman, F.J.R., et al., 2003. Relations between local, nonlocal, discrete and continuous models of bioturbation. J. Mar. Res. 61, 391-410.

Michel, H.V., et al., 1991. Geochemical study of the Cretaceous-Tertiary boundary region at Hole 752B. Proc. Ocean Drill. Prog. Sci. Results 121, 415-422.

Michel, H.V., et al., 1981. Distribution of iridium and other elements near the Cretaceous/Tertiary boundary in Hole 465A: preliminary results. Init. Repts. Deep Sea Drill. Prog. 62, 847-849.

Michel, H.V., et al., 1985. Elemental profile of iridium and other elements near the Cretaceous/Tertiary boundary in Hole 577B. Init. Repts. Deep Sea Drill. Prog. 86, 533-538.

Michel, H.V., et al., 1990. Geochemical studies of the Cretaceous-Tertiary boundary in ODP holes 689B and 690C. Proc. Ocean Drill. Prog. Init. Repts. 113, 159-168.

Officer, C.B., Drake, C.L., 1983. The Cretaceous-Tertiary transition. Science 219, 1383-1390.

Officer, C.B., Drake, C.L., 1985. Terminal Cretaceous environmental events. Science 227, 1161-1167.

Paquay, F.S., et al., 2008. Determining chondritic impactor size from the marine osmium isotope record. Science 320, 214-218.

Perch-Nielsen, K., et al., 1977. Site 356: São Paulo Plateau. Init. Repts. Deep Sea Drill. Prog. 39, 141-230.

Pospichal, J.J., 1994. Calcareous nannofossils at the K-T Boundary, El Kef - no evidence for stepwise, gradual, or sequential extinctions. Geology 22, 99-102.

Pospichal, J.J., et al., 1990. The effects of bioturbation across a biostratigraphically complete high southern latitude Cretaceous/Tertiary boundary. Geol. Soc. Am. Spec. Pap. 247, 497-507.

Preisinger, A., et al., 1986. The Cretaceous Tertiary Boundary in the Gosau Basin, Austria. Nature 322, 794-799.

Premoli Silva, I., et al., 2005. Data Report: Planktonic foraminiferal biostratigraphy across the Cretaceous/Paleocene boundary at Shatsky Rise (ODP Leg 198, Northwest Pacific). Proc. Ocean Drill. Prog. Sci. Results 198, 1-16.

Ravizza, G., Peucker-Ehrenbrink, B., 2003. Chemostratigraphic evidence of Deccan volcanism from the marine osmium isotope record. Science 302, 1392-1395.

Robin, E., et al., 1991. The Stratigraphic distribution of Ni-rich spinels in Cretaceous-Tertiary boundary rocks at El-Kef (Tunisia), Caravaca (Spain) and Hole-761c (Leg-122). Earth Planet. Sci. Lett. 107, 715-721.

Robinson, N., et al., 2009. A high-resolution marine Os-187/Os-188 record for the late Maastrichtian: distinguishing the chemical fingerprints of Deccan volcanism and the KP impact event. Earth Planet. Sci. Lett. 281, 159-168.

Rocchia, R., et al., 1992. Iridium and other element distributions, mineralogy, and magnetostratigraphy near the Cretaceous/Tertiary Boundary in Hole 761C. Proc. Ocean Drill. Prog. Sci. Results 122, 753-762.

Rocchia, R., et al., 1990. The Cretaceous Tertiary boundary at Gubbio revisited - vertical extent of the Ir anomaly. Earth Planet. Sci. Lett. 99, 206-219.

Rodriguez-Tovar, F., Uchman, A., 2008. Bioturbational disturbance of the Cretaceous-Palaeogene (K-Pg) boundary layer: implications for the interpretation of the K-Pg boundary impact event. Geobios 41, 661-667.

Rodriguez-Tovar, F.J., 2005. Fe-oxide spherules infilling Thalassinoides burrows at the Cretaceous-Paleogene (K-P) boundary: evidence of a near-contemporaneous macrobenthic colonization during the K-P event. Geology 33, 585-588.

Ross, O.N., Sharples, J., 2004. Recipe for 1-D Lagrangian particle tracking models in space-varying diffusivity. Limnol. Oceanogr.: Methods 2, 289-302.

Ruddiman, W.F., Glover, L.K., 1972. Vertical mixing of ice-rafted volcanic ash in North Atlantic sediments. Geol. Soc. Am. Bull. 83, 2817-2835.

Ruddiman, W.F., et al., 1980. Tests for size and shape dependency in deep-sea mixing. Sediment. Geol. 25, 257-276.

Sawlowicz, Z., 1993. Iridium and other Platinum-Group Elements as geochemical markers in sedimentary environments. Palaeogeogr. Palaeoclimatol. Palaeoecol. 104, 253-270.

Schmitz, B., 1985. Metal precipitation in the Cretaceous-Tertiary boundary clay at Stevns Klint, Denmark. Geochim. Cosmochim. Acta 49, 2361-2370.

Schmitz, B., et al., 1991. Element stratigraphy across the Cretaceous/Tertiary bounadry in Hole 738C. Proc. Ocean Drill. Prog. Sci. Results 119, 719-730.

Schulte, P., et al., 2010. The Chicxulub Asteroid Impact and Mass Extinction at the Cretaceous-Paleogene Boundary. Science 327, 1214-1218.

Shull, D.H., 2001. Transition-matrix model of bioturbation and radionuclide diagenesis. Limnol. Oceanogr. 46, 905-916.

Smit, J., 1999. The global stratigraphy of the Cretaceous-Tertiary boundary impact ejecta. Annu. Rev. Earth Planet. Sci. 27, 75-113.

Smit, J., et al., 1996. Coarse-grained, clastic sandstone complex at the K/T boundary around the Gulf of Mexico: deposition by tsunami waves induced by the Chicxulub impact? Geol. Soc. Am. Spec. Pap. 307, 151-182.

Smith, C.R., Rabouille, C., 2002. What controls the mixed-layer depth in deep-sea sediments? The importance of POC flux. Limnol. Oceanogr. 47, 418-426.

Smith, J.N., et al., 1986. Plutonium and ^{210}Pb distributions in northeast Atlantic sediments: subsurface anomalies caused by non-local mixing. Earth Planet. Sci. Lett. 81, 15-28.

Stuben, D., et al., 2002. Two anomalies of platinum group elements above the Cretaceous-Tertiary boundary at Beloc, Haiti: Geochemical context and consequences for the impact scenario. Geol. Soc. Am. Spec. Pap. 356, 55-68.

Stuben, D., et al., 2005. High-resolution geochemical record of Cretaceous-Tertiary boundary sections in Mexico: New constraints on the K/T and Chicxulub events. Geochim. Cosmochim. Acta 69, 2559-2579.

Stueben, D., et al., 2002. Two anomalies of platinum group elements above the Cretaceous-Tertiary boundary at Beloc, Haiti: Geochemical context and consequences for the impact scenario. Geol. Soc. Am. Spec. Pap. 356, 55-68.

Tada, R., et al., 2002. Complex tsunami waves suggested by the Cretaceous-Tertiary bounary deposit at the Moncada section, western Cuba. Geol. Soc. Am. Spec. Pap. 356, 109-123.

Tanaka, Y., Franks, P.J.S., 2008. Vertical distributions of Japanese sardine (Sardinops melanostictus) eggs: comparison of observations and a wind-forced Lagrangian mixing model. Fish. Oceanogr. 17, 89-100.

Thierstein, H.R., 1981. Late Cretaceous calcareous nannoplankton and the change at the Cretaceous-Tertiary boundary. Spec. Publ.—Soc. Econ. Paleontol. Mineral. 32, 355-394.

Thomson, J., et al., 1995. Radiocarbon age offsets in different-sized carbonate components of deep-sea sediments. Radiocarbon 37, 91-101.

Trauth, M.H., 1998. TURBO: A dynamic-probabilistic simulation to study the effects of bioturbation on paleoceanographic time series. Comput. Geosci. 24, 433-441.

Trauth, M.H., et al., 1997. Bioturbational mixing depth and carbon flux at the seafloor. Paleoceanography 12, 517-526.

Vallier, T.L., et al., 1981. Site 465: Southern Hess Rise. Init. Repts. Deep Sea Drill. Prog. 62.

Visser, A.W., 1997. Using random walk models to simulate the vertical distribution of particles in a turbulent water column. Mar. Ecol. Prog. Ser. 158, 275-281.

Wallace, M.W., et al., 1990. Acraman impact ejecta and host shales - evidence for low-temperature mobilization of iridium and other platinoids. Geology 18, 132-135.

Wang, K., et al., 1993. Global iridium anomaly, mass extinction, and redox change at the Devonian-Carboniferous boundary. Geology 21, 1071-1074.

Westerhold, T., et al., 2008. Astronomical calibration of the Paleocene time. Paleogeogr. Paleoclimatol. Paleoecol. 257, 377-403.

Wheatcroft, R.A., 1992. Experimental tests for particle size-dependent bioturbation in the deep ocean. Limnol. Oceanogr. 37, 90-104.

Figure Captions

Figure 1. The Lagrangian sediment mixing model. Three mixing curves highlight the effect of z_{scale} on depth-dependent diffusivity (K_v). All curves are parameterized with the same z_0, indicated on the depth axis, and the same K_0. Larger values for z_{scale} (black) increase the depth range over which K_v asymptotes to zero relative to a smaller z_{scale} values (grey).

Figure 2. Theoretical examples of the effect of mixing parameters on model iridium profile shape. A standard mixing model (K_0= 1.0 cm^2/kyr, z_0= 5 cm, z_{scale}= 1.5 cm, (w_s)= 0.5 cm/kyr, single input of 100,000 tracer particles at time zero) was used to illustrate the model sensitivity to changes in (a) sediment diffusivity, K_0, (b) sedimentation rate, w_s, and (c) the depth of the well-mixed zone, (z_0). Different model parameterizations are shown in each panel (a-f) with solid to dotted and black or grey lines (see panel specific legends for details). (d) Three scenarios for a prolonged iridium injection are shown assuming no sediment mixing and an iridium oceanic residence time of 6.3 kyr (10 and 30% impactor dissolution) or 20 kyr (70% dissolution). (e) Mixing scenario 1 contrasts the standard mixing model with and without a prolonged input of iridium from an assumed 30% impactor dissolution and 6.3 kyr residence time. Rectangles indicate samples used to calculate r^2. (f) Mixing scenario 2 contrasts the standard mixing model against a scenario assuming prolonged iridium deposition and elevated sediment mixing (depth and rate) for a short period following the K-Pg impact. In all cases, modeled concentrations were scaled to a peak tracer concentration of 100 and centered to peak concentration depth equal to 0 cm. This procedure mirrors the fitting of empirical profiles (where initial magnitude and depth are considered unknowns) but obscures important

differences in the depth of the peak shift and the absolute anomaly magnitude with different model parameterizations.

Figure 3. Core photographs illustrate sediment mixing of sediment at Maud Rise and Hess Rise. Iridium anomalies are plotted adjacent to photographs of cores for (a) the heavily bioturbated Maud Rise KPg boundary (Barker et al. 1988, Michel et al. 1990), and (b) the coring-disturbed KPg boundary at Hess Rise (Michel et al. 1981, Vallier et al. 1981).

Figure 4. Iridium anomalies from three regions illustrate the effects of lumpy mixing and sedimentary disturbance on anomaly shape. Iridium anomalies from sites in (a) the Indian (Michel et al. 1991, Schmitz et al. 1991, Rocchia et al. 1992) and (b) the Pacific Ocean (Michel et al. 1985, Kyte et al. 1995) show differences in anomaly shape and small secondary peaks, likely due to lumpy mixing. (c) Multiple peaks and large iridium anomaly shape differences between sites in the Gulf of Mexico (Smit et al. 1996, Stuben et al. 2002, Tada et al. 2002) likely reflect high-energy sediment transport from tsunamis, gravity flows, and near-impact forces (Schulte et al. 2010). Individual iridium records within each basin are indicated with black, grey, and black dotted lines (a-c, see panel specific legends for details). In all cases, iridium concentrations were scaled to a maximum concentration of 100 and centered to peak concentration depth equal to 0 cm, obscuring differences the magnitude of the absolute iridium anomaly and peak offset from the biostratigraphic K-Pg boundary.

Figure 5. Investigation of potential mechanisms leading to iridium anomaly shape at DSDP 577B, Shatsky Rise using the Lagrangian particle sediment mixing model. The 577B iridium anomaly is plotted against (a) elements ranging in redox sensitivity, (b) a model of prolonged iridium deposition assuming no mixing, (c) a model of iridium

mixing assuming a near one-layer mixing profile (K_0=0.75 cm^2/kyr, z_0=19.8 cm, and z_{scale}=1.5 cm), and (d) a model of iridium mixing assuming an asymptotic decrease in sediment mixing with depth (K_0= 1.92 cm^2/kyr, z_0= 9.1 cm, and z_{scale}= 7.1 cm). Both mixing models (c-d) performed equally well (r^2= 0.95 and p< 0.001), with the simpler model (c) providing the best model fit relative to model complexity. All models (b-d) assume that 90% of iridium was deposited instantaneously and 10% was impact-vaporized with an oceanic residence time of 6,300 years. In all panels iridium is plotted with dark grey circles; in panels b-d the open, light grey circles indicate iridium samples that were excluded from the calculation of r^2. In panels b-d the median sedimentary model is represented by a black line; light grey shading in c & d indicates the 5th and 95th percentile model run values.

Figure 1.

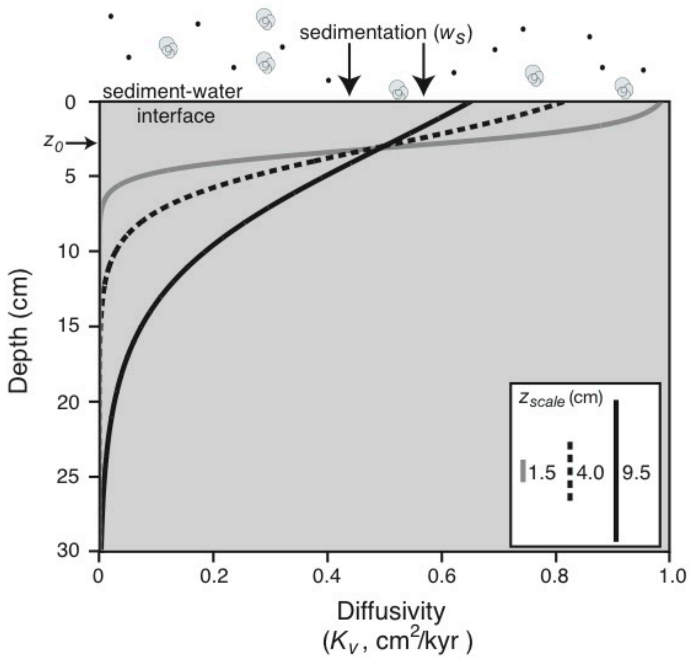

sedimentation (w_S)
sediment-water
interface
0
z_0
5
10
15
20
25
30
Depth (cm)
0
0.2
0.4
0.6
0.8
1.0
Diffusivity
(K_v, cm^2/kyr)
z_{scale} (cm)
1.5
4.0
9.5

Figure 2.

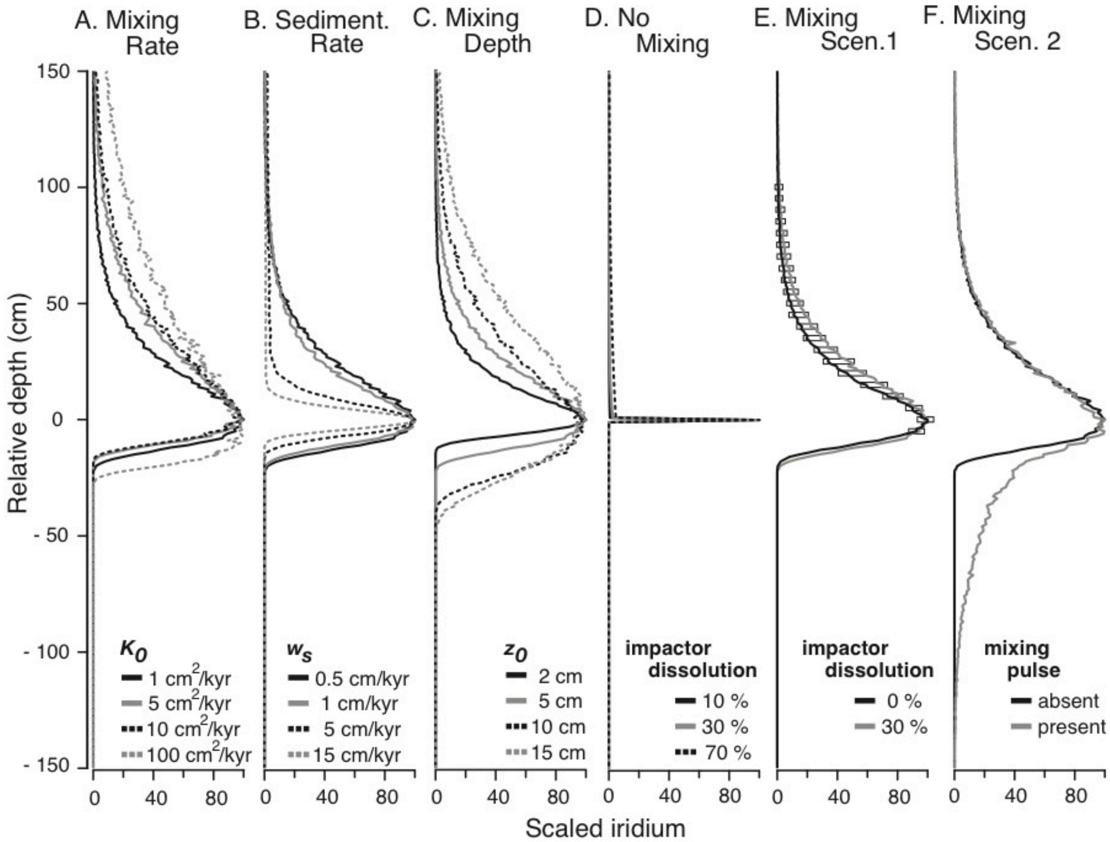
A. Mixing Rate
B. Sediment. Rate
C. Mixing Depth
D. No Mixing
E. Mixing Scen.1
F. Mixing Scen. 2
Relative depth (cm)
150
100
50
0
- 50
- 100
- 150
κ_0
1 cm^2/kyr
5 cm^2/kyr
10 cm^2/kyr
100 cm^2/kyr
w_s
0.5 cm/kyr
1 cm/kyr
5 cm/kyr
15 cm/kyr
z_0
2 cm
5 cm
10 cm
15 cm
impactor dissolution
10 %
30 %
70 %
impactor dissolution
0 %
30 %
mixing pulse
absent
present
0
40
80
Scaled iridium

Figure 3.

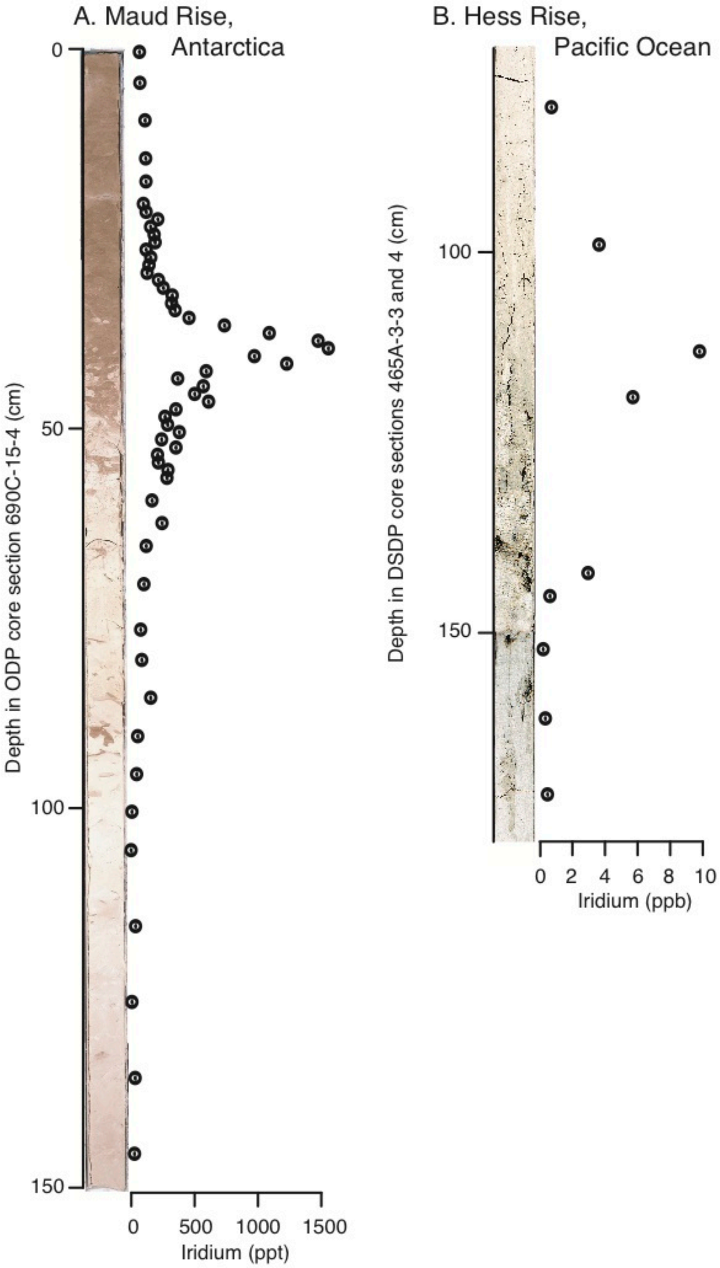
A. Maud Rise,
Antarctica
Depth in ODP core section 690C-15-4 (cm)
0
50
100
150
0
500
1000
1500
Iridium (ppt)
B. Hess Rise,
Pacific Ocean
Depth in DSDP core sections 465A-3-3 and 4 (cm)
100
150
0
2
4
6
8
10
Iridium (ppb)

Figure 4.

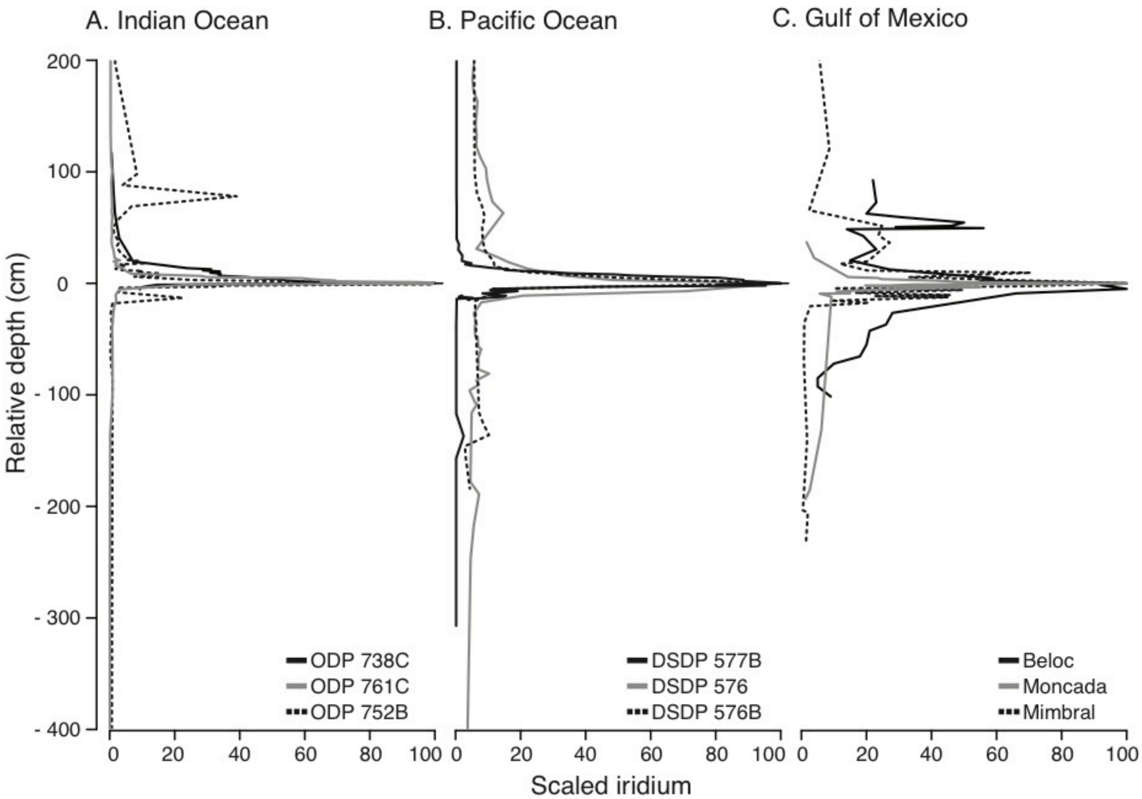
A. Indian Ocean
B. Pacific Ocean
C. Gulf of Mexico
Relative depth (cm)
Scaled iridium
ODP 738C
ODP 761C
ODP 752B
DSDP 577B
DSDP 576
DSDP 576B
Beloc
Moncada
Mimbral
200
100
0
- 100
- 200
- 300
- 400
0
20
40
60
80
100

Figure 5.

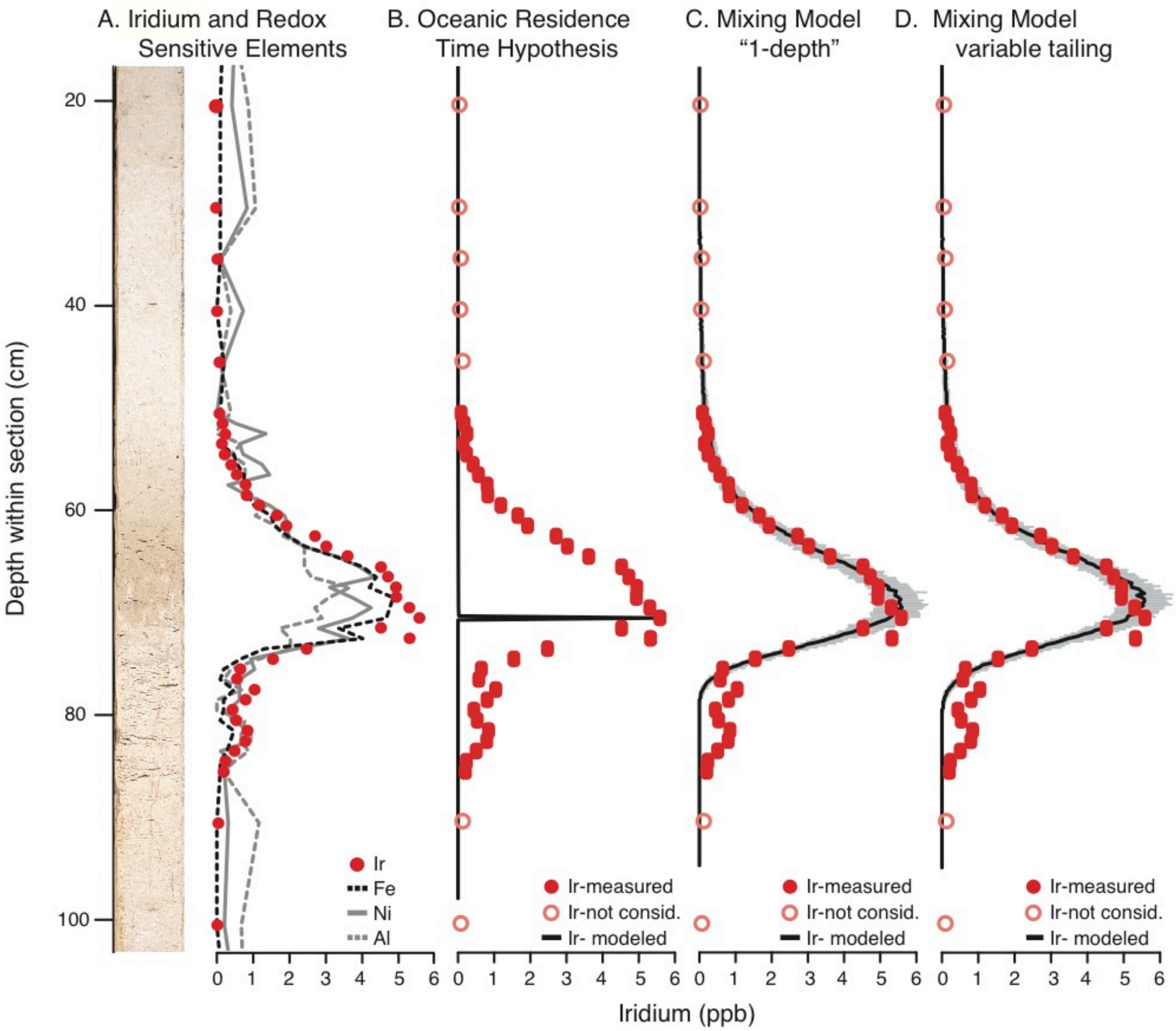
A. Iridium and Redox
Sensitive Elements
B. Oceanic Residence
Time Hypothesis
C. Mixing Model
"1-depth"
D. Mixing Model
variable tailing
Depth within section (cm)
20
40
60
80
100
Ir
Fe
Ni
Al
Ir-measured
Ir-not consid.
Ir- modeled
0 1 2 3 4 5 6
Iridium (ppb)